

Verification of atomic data for solar oxygen abundance models

Sultana N. Nahar[★]

Department of Astronomy, The Ohio State University, Columbus, OH 43210, USA

Accepted 2022 February 11. Received 2022 February 11; in original form 2021 November 29

ABSTRACT

Recently, Bergemann et al. reported a re-analysis of O I lines, 777 and 630 nm, using their new atomic models of O and Ni, and presented solar photospheric oxygen abundance differing from others. We discuss the accuracy of atomic data employed in their models, and demonstrate that the photoionization cross-sections (σ_{PI}) of the two levels $1s^2 2s^2 2p^3 3s(^5S_2^o)$ and $1s^2 2s^2 2p^3 3p(^5P_1)$, which they present as illustrations of their data in the non-local-thermodynamic-equilibrium (NLTE) model, are incorrect by large factors. For example, their σ_{PI} at the threshold of level $^5S_2^o$ is larger by a factor of 1000 than that of Nahar and the Opacity Project data base, TOPbase, and has an incorrect energy behaviour. They included a blending of the 630 nm line with Ni I for which they computed σ_{PI} in the hydrogenic approximation. The approximation does not include electron–electron interaction and hence is not valid for Ni I. They noted that the use of oscillator strengths of O I by Hibbert et al., which agree very well with TOPbase and Nahar, gave an abundance close to the existing values, but reported using averaged values of two sources. Therefore, their oxygen abundance from the new atomic models is likely to be in question.

Key words: atomic data – atomic processes – line: identification – opacity – Sun: abundances – Sun: photosphere.

1 INTRODUCTION

Owing to its high abundance in the Sun and the Universe, oxygen has been extensively investigated. The Sun is the standard for studying other stellar systems, implying that accurate solar abundances will reduce uncertainties in those derived for other stars. Determination of solar elemental abundances has remained a long-standing problem, largely due to the lack of complete sets of consistent and accurate data for the atomic processes involved in spectral lines formation and issues in describing proper plasma conditions in the non-local-thermodynamic-equilibrium (NLTE) models employed. Asplund et al. (2021) have essentially reconfirmed solar abundances derived from their three-dimensional (3D) NLTE model, with particular focus on oxygen, and discuss recent works by Amarsi et al. (2018) and Caffau et al. (2015). Bergemann et al. (2021; hereafter B21) also carried out another re-analysis using their new atomic models of O and Ni and reported significant differences from Asplund et al. (2021). In this Letter, we examine the accuracy of the atomic data employed and differences with previous results not considered by B21.

Two spatially resolved diagnostic lines of O I, 777 and 630 nm, of the Sun, detected with high-resolution, $R \approx 700\,000$ with the IAG FTS instrument, were analysed by B21. While the 777 nm line is due to a dipole that allowed E1 transition between two excited states $2s^2 2p^3(^4S^o) 3s^5S^o$ and $2s^2 2p^3(^4S^o) 3p^5P$, the 630 nm is a forbidden line associated with E2 and M1 transitions within the ground configuration $1s^2 2s^2 2p^4$ of O I. Table 1 presents the levels and fine structure components of these lines, and also shows that the O I 630 nm line can be blended with a 630 nm line formed from an E1 transition between two excited levels of Ni I.

B21 analysed the 777 nm line of O I using a 1D NLTE hydrostatic model and the 630 nm line using a 3D hydrodynamical model to determine the solar photospheric oxygen abundance $A(O)$. They emphasized the 630 nm line of O I accounting for the Ni I blend (Table 1). With their new atomic models for O and Ni, they derive $\log A(O) = 8.75 \pm 0.03$, which is close to but differs significantly from values obtained by others, such as 8.69 ± 0.04 dex by Asplund et al. (2021).

Their new atomic models for O and Ni include photoionization cross-sections (σ_{PI}) of O I and Ni I. They particularly describe photoionization cross-sections (σ_{PI}) of O I for the 3D non-LTE study of the spectral line to derive the oxygen abundance. They report the computation of σ_{PI} for O I using the package of programmes (Berrington et al. 1995) of the Breit–Pauli R-Matrix (BPRM) method as developed by the Opacity Project (OP, The Opacity Project Team, 1995) and the Iron Project (IP, Hummer et al. 1993). These data are expected to be accurate. However, the data they present are inconsistent and inaccurate for the O I lines of interest. For σ_{PI} of Ni I, they used the hydrogenic approximation, which is not valid since the approximation does not represent electron–electron correlation effects to produce autoionizing resonances that are present in complex atomic systems. This report aims to highlight the importance of the accuracy verification of atomic parameters that go into the plasma model calculations for the determination of elemental abundances. It does not quantify the contributions of the processes in the model since those depend on how the model represents the environment.

Photoionization cross-sections for O I using the R-matrix method were obtained under the OP by Butler and Zeippen and are available on OP data base TOPbase (Cunto and Mendoza 1992), and later by Nahar (1998, hereafter N98) and are available on the data base NORAD-Atomic-Data (NORAD, Nahar 2020). Both calculations are independent of each other and use different sizes of close coupling

[★] E-mail: nahar@astronomy.ohio-state.edu, nahar.1@osu.edu

Table 1. Observed lines of O I (777 nm, 630 nm) and Ni I (631 nm) in the solar photosphere.

Transition	$\lambda(\text{\AA})$	Type
O I		
$2s^2 2p^3 ({}^4S^o) 3s^5 S_2^o - 2s^2 2p^3 ({}^4S^o) 3p^5 P_3$	7771.940	E1
$2s^2 2p^3 ({}^4S^o) 3s^5 S_2^o - 2s^2 2p^3 ({}^4S^o) 3p^5 P_2$	7774.170	E1
$2s^2 2p^3 ({}^4S^o) 3s^5 S_2^o - 2s^2 2p^3 ({}^4S^o) 3p^5 P_1$	7775.390	E1
$2s^2 2p^4 {}^3P_2 - 2s^2 2p^4 ({}^1D)_2$	6300.304	E2
$2s^2 2p^4 {}^3P_2 - 2s^2 2p^4 ({}^1D)_2$	6300.304	M1
Ni I		
$3d^8 4s 4p^3 D_1^o - 3d^8 ({}^1S_0) 4s^2 {}^1S_0$	6300.341	E1

wavefunction expansions. N98 data are an improvement over the OP data and are for a larger number of excited bound states. N98 considered more dipole allowed excitations of the core ion O II than Butler and Zeippen. This resulted in many more resonances caused by core ion excitations than those in TOPbase. B21 compared O I σ_{PI} with those in TOPbase obtained by Butler and Zeippen but did not compare with or refer to those of N98.

2 ATOMIC PROCESSES AND PARAMETERS FOR SPECTRAL ANALYSIS AND ABUNDANCES

Spectral lines in astrophysical plasmas form due to five dominant atomic processes that involve a photon: (i) photo-excitations or de-excitation, (ii) photoionization (PI), (iii) electron-ion recombination (RC), (iv) electron-impact excitation (EIE), and (v) hydrogen collision for transitions and other processes. Line intensity also depends on the other dominant process of electron impact ionization (EII). The dominance of these processes depends on the plasma environment consisting of temperature, density, radiation field, etc. In solar photosphere, hydrogen colliding with neutral atoms is an important process, while collisions with electrons are not important because of the lack of electrons. Characteristic features of atomic processes, revealed by corresponding atomic parameters, provide information that affects applications such as determination of elemental abundances in the plasma. The precision of NLTE models typically depends on the accuracy of atomic parameters in the relevant abundance equations and also on the accuracy of the plasma model describing the impact of plasma environment on the atomic processes and parameters. A detailed description on the study of the parameters and modelling can be found in Pradhan and Nahar (2011) and Hubeny and Mihalas (2014).

B21 used various sources for the data of the atomic processes and discussed the details of the data, such as oscillator strengths for photo-excitations, collision strengths, excitation and ionization cross-sections, photoionization cross-sections, etc.

3 RESULTS AND DISCUSSION

With the exception of photoionization cross-sections of O I using the BPRM method, B21 computed other atomic data using simple approximations and used those from other sources for their new atomic models.

For oscillator strengths (f-values) of O I lines, they chose to use the average values of those of Hibbert et al. (1991) obtained in configuration interaction calculations and of Civiš et al. (2018) obtained in a single electron quantum defect method for the three 777 nm lines and Storey & Zeippen (2000) data for the 630 nm lines. For other transition parameters of O I, O II, Ni I, Ni II, they include data from various sources, including large sets of data from the Kurucz

data base (<http://kurucz.harvard.edu/atoms/0800/>). Their model is dependent on the values of the oscillator strengths of O I. They found that using the Hibbert et al. (1991) f-values for the 777 nm lines and the SST observed data, their results based on the LCAO + K model atom of O were in excellent agreement with the 3D NLTE estimate by Amarsi et al. (2018), who used the same input as theirs, and their 1D NLTE result based on the MARCS model would agree with that of Sitnova & Mashonkina (2018). The accuracy of Hibbert et al. (1991) f-values is high since their multiplet value of 1.008 is in excellent agreement, within 3 per cent, with 0.9776 of the OP and 0.9818 of N98. However, B21 used the average value of two separate sources that appeared to give different abundances than others.

For H collisions with O I, including both the elastic and inelastic scatterings, the collisional rate coefficients and the transition rates they included were obtained largely by Barklem and collaborations, and by some others (references in B21).

For electron impact excitations for O I, B21 computed the rate coefficients for a number of low-lying excited levels using single-channel distorted wave approximation built-in programme AUTOSTRUCTURE. They wrongly quote these values as results from the R-matrix method. The R-matrix method, in contrast to the distorted wave approximation, is a multi-channel coupling approximation that can produce much more accurate values, as were obtained by Tayal and Zatsarinny (2016) and were implemented by Amarsi et al. (2018) for their oxygen abundance calculations. For the remainder of the levels, B21 used the simple van Regemorter formula (1962) that is largely uncertain as it is generally accurate only to a factor of 2 or 3 (Seaton 1975).

For H and electron collisions with Ni, they calculated the rates of collisional excitation using simple formulas of van Regemorter (1962) and Drawin (1968), but scaled the rates by a factor of 0.05 for the collisions of Ni I atoms with H by explaining that these formulas are known to overestimate rate coefficients compared to the detailed quantum-mechanical data. They used the Seaton (1962) formula for rates for collisional ionization of Ni I.

In particular, the newly computed photoionization cross-sections (σ_{PI}) by B21 for O I are incorrect and hydrogenic cross-sections for Ni I are invalid. B21 carried out BPRM calculations for σ_{PI} for O I using the R-matrix programmes (Berrington et al. 1987; 1995) but do not provide any evidence of the accuracy of data, such as by comparing their energy values with those at NIST or comparing the ground state photoionization with experimental data which are available. Both Butler and Zeippen (1990) and N98 benchmarked their σ_{PI} for the ground state of O I with measured data. The description of BPRM calculation for O I by B21 is also not clear. They mention considering 11 configurations (which has a typo, specifying 3p in place of 2p) for the core ion O II and using 26 terms for 39 energy levels going up to $n = 20$. These do not seem to be correct since the NIST compilation table does not show that the lowest 39 levels go up to $n = 20$. We discuss σ_{PI} that B21 has presented for the two excited levels, $2s^2 2p^3 3s ({}^5S_2^o)$ and $2s^2 2p^3 3p ({}^5P_1)$, which form the 777 nm line via radiative transitions, and demonstrate that their O I cross-sections are incorrect.

Fig. 1 presents σ_{PI} of the $2p^3 3s ({}^5S^o)$ state of O I: the left subplot shows σ_{PI} from B21 (solid curve), which is being compared with those of Butler and Zeippen (TOPbase, dash curve), and the right subplot shows the same σ_{PI} obtained by Butler and Zeippen on the top panel and σ_{PI} by N98 in the lower panel. Both the TOPbase and N98 agree with each other in shape and features of σ_{PI} , except for additional resonances and enhanced background in N98, beyond those in TOPbase. The features between 600 and 500 Å in N98 are contributions from additional core ion excitations included in the

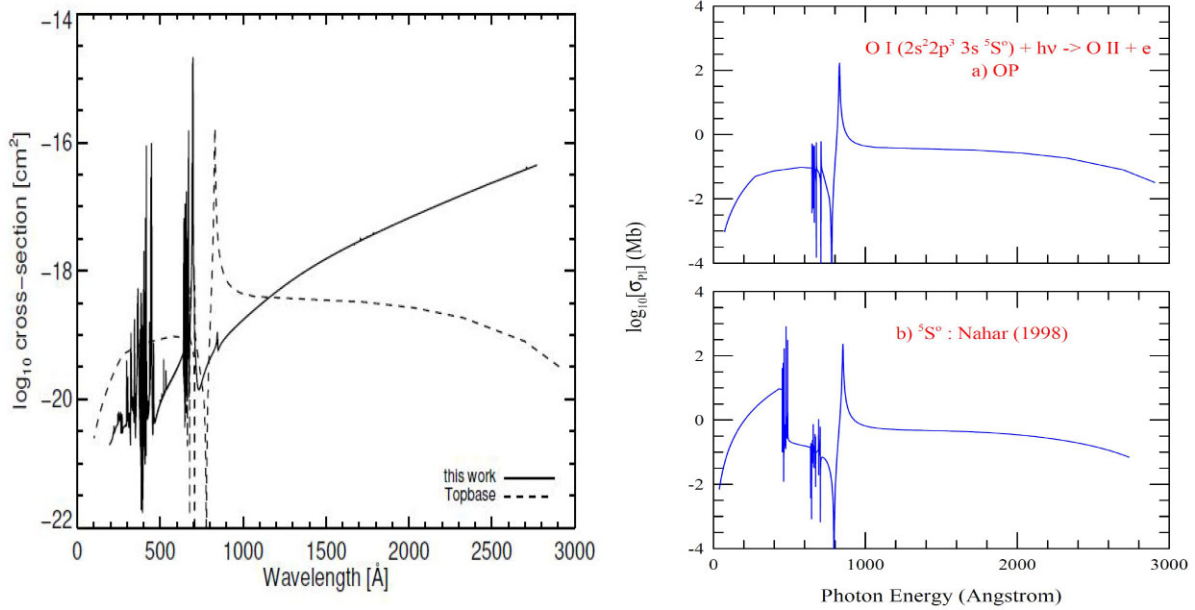


Figure 1. Photoionization cross-section σ_{PI} of the excited $2s^2 2p^3 3s(^5S^o)$ state of O I. Left-hand panel: solid curve: **B21**; dashed curve: Butler and Zeippen available at TOPbase. Upper right-hand panel: TOPbase data of Butler and Zeippen; lower right-hand panel: **N98**. The features of σ_{PI} available from TOPbase and **N98** agree except for more resonances in **N98** from consideration of additional core ion excitations. **B21** show completely different resonant features and a threshold cross section that is 1000 times higher than TOPbase and **N98**.

calculations. **B21** shows different shape and features. The cross-section in both TOPbase and **N98** starts with a large resonance with a rising trend from the ionization threshold. In **N98**, a similar shaped resonance appears just below 500 Å indicating it belongs to the same series as the first resonance. In contrast to the rising resonance, **B21** shows a decreasing trend for σ_{PI} starting from a high value, 1000 times higher than that of the TOPbase and of **N98**, at the threshold. The TOPbase σ_{PI} starts at an energy lower than that in **N98** as it tabulates additional points below the ionization threshold that are needed for the opacity calculations. Both TOPbase and **N98** show σ_{PI} at higher energy, beyond the resonances of the highest core excitation at wavelengths 300 Å and smaller, a similar decreasing trend. These σ_{PI} values were obtained using Kramers formula, an approach adopted under the OP, for high energy behaviour of σ_{PI} . Compared to TOPbase and **N98**, **B21** shows a completely different shape and features in σ_{PI} of $^5S^o$ state.

To resolve the large discrepancy at threshold of rising trend resonance and decreasing, features of an O I electronic sequence ion can be studied. These ions with the same number of electrons generally demonstrate similar characteristic features in σ_{PI} . Fig. 2 presents σ_{PI} of ($^5S^o$) of Ne III, isoelectronic to O I with eight electrons and same electronic structure. $\sigma_{PI}(^5S^o)$ of Ne III was obtained using the BPRM method (Nahar 2019) that **B21** also used for O I but using a larger wavefunction expansion. There are differences between O I and Ne III. Ne III is more highly charged than neutral O I which generally causes shifting and compression of the resonances. However, O I and Ne III also show general similarities. Similar to O I of **N98**, σ_{PI} of ($^5S^o$) state of Ne III starts with a characteristic resonance series where the first one is a large resonance at the ionization threshold and the second one is at ~ 2.75 Ry with a similar shape. The first resonance is exhibiting a rising trend at the ionization threshold supporting the similar one in the predicted σ_{PI} of O I by **N98** and TOPbase, and contradicting the decreasing values from threshold of **B21**. These features of the $^5S^o$ state of Ne III, and hence of O I, are further

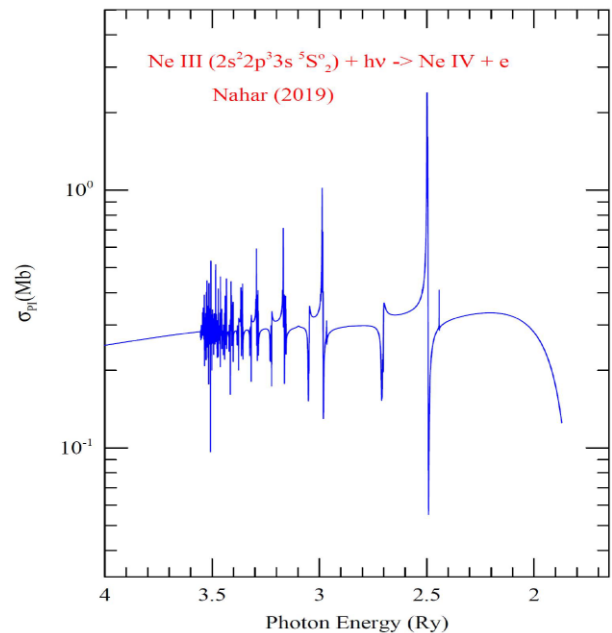


Figure 2. Photoionization cross-section σ_{PI} of the excited $2s^2 2p^3 3s(^5S^o)$ state of Ne III (Nahar 2019) isoelectronic to O I. Ne III verifies similar general features of the same state of O I (Nahar 1998) and a rising resonance at the ionization threshold.

confirmed to be correct as the σ_{PI} of Ne III measured at the Advanced Light Source (ALS) of synchrotron set-up at the Lawrence Berkeley National Laboratory was benchmarked by Nahar et al. (2019). Thus, Ne III re-confirms that $\sigma_{PI}(^5S^o)$ of O I in **B21** is inaccurate.

$2s^2 2p^3 3p(^5P_1)$ is the only other level for which **B21** present σ_{PI} (Figure 3, the solid curve in the left-hand subplot) and compare with TOPbase data (dashed curve). **B21** find more resonances than

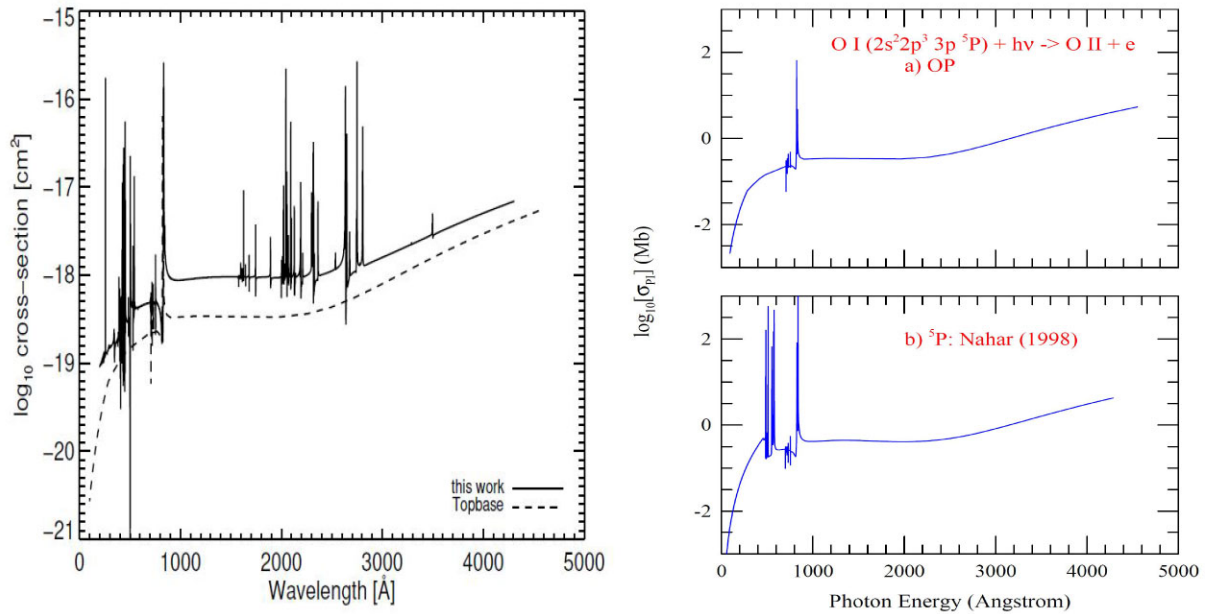


Figure 3. Photoionization cross-section σ_{PI} of the excited $2s^2 2p^3 3p^5 P$ state of O I. Left-hand panel: solid curve: **B21**; dashed curve: TOPbase data by Butler and Zeippen, Upper right-hand panel: same TOPbase data by Butler and Zeippen; lower right-hand panel: **N98**. The features of σ_{PI} from TOPbase and **N98** agree with each other except for additional resonances in **N98** from core excitations. **B21** show features and background cross-section different from both.

TOPbase does. The right subplot presents the same TOPbase cross-sections on the top panel and those of **N98** in the lower panel which agree with each other in features. The only differences between TOPbase and **N98**, which are similar to those of $2s^2 2p^3 3s^5 S^o$ described above, are: (i) **N98** has more resonances due to inclusion of additional core ion excitations, (ii) TOPbase starts at lower energy because of additional points below the ionization threshold, and (iii) **N98** resolved resonances with a finer energy mesh, resulting in higher peaks than those in TOPbase. All three sets of results (**B21**, TOPbase, and **N98**) presented in Figure 3 were carried out using the same R-matrix package of codes developed under the OP (The Opacity Project Team 1995) and the IP (Hummer et al. 1993), and hence are expected to be similar. However, compared to the two separate computations with different wavefunction expansions by Butler and Zeippen and by **N98**, which agree with each other, **B21** show very different features that are incorrect.

Explanation of justification or emphasis of their calculations of new photoionization data of O I (which are apparently incorrect) up to $n = 20$, number of energy states, inclusion of relativistic effects, and use of fine energy grid seem redundant since **B21** includes data in their model up to $n = 5$ and a minimum number of points that do not include resonances. For such a purpose, the use of the OP data would have been more than adequate.

These discussions establish the fact that the new atomic models of **B21** contains inconsistent and inaccurate photoionization cross-sections of O I and Ni I and indicate uncertainty in their results.

4 CONCLUSION

As discussed in detail in this Letter, the **B21** model for solar oxygen abundance is shown to be uncertain owing to inaccurate atomic data, and consequent uncertainty in their value for the abundance.

ACKNOWLEDGEMENTS

The author would like to thank Anil Pradhan for discussions. She also acknowledges the in-depth knowledge of the referee on the topic and that he/she provided useful and detailed remarks. The computational work was carried out at the Ohio Supercomputer Center in Columbus, Ohio.

DATA AVAILABILITY

All atomic data presented here from the author are available at the online data base NORAD-Atomic-Data at <http://norad.astronomy.ohio-state.edu>

REFERENCES

- Amarsi A. M., Barklem P. S., Asplund M., Collet R., Zatsarinny O., 2018, *A&A*, 616, A89
- Asplund M., Amarsi A. M., Grevesse N., 2021, *A&A*, 653, A141
- Bergemann M. et al., 2021, *MNRAS*, 508, 2236 (B21)
- Berrington K. A., Burke P. G., Butler K., Seaton M. J., Storey P. J., Taylor K. T., Yan Yu., 1987, *J. Phys. B*, 20, 6379
- Berrington K. A., Eissner W., Norrington P. H., 1995, *Comput. Phys. Commun.*, 92, 290
- Butler K., Zeippen C. J., 1990, *A&A*, 234, 569
- Caffau E., Ludwig H. G., Steffen M., Livingston W., Bonifacio P., Malherbe J. M., Doerr H. P., Schmidt W., 2015, *A&A*, 579, A88
- Civiš S., Kubelík P., Ferus M., Zanozina E. M., Pastorek A., Naskidashvili A. V., Chernov V. E., 2018, *ApJS*, 239, 11
- Cunto W., Mendoza C., 1992, *Rev. Mex. Astron. Astrofis.*, 23, 107
- Drawin H.-W., 1968, *Z. Phys.*, 211, 404
- Hibbert A., Biemont E., Godefroid M., Vaecek N., 1991, *J. Phys. B*, 24, 3943
- Hubeny I., Mihalas D., 2014, *Theory of Stellar Atmospheres: An Introduction to Astrophysical Non-Equilibrium Quantitative Spectroscopic Analysis*. Princeton Univ. Press, Princeton, NJ

- Hummer D.G., Berrington K. A., Eissner W., Pradhan A. K., Saraph H. E., Tully J. A., 1993, *A&A*, 279, 298
- Nahar S. N., 1998, *Phys. Rev. A*, 58, 3766 (N98)
- Nahar S. N., 2019, *New Astron.*, 67, 97
- Nahar S. N., 2020, *Atoms*, 8, 68
- Nahar S. N. et al., 2019, *J. Mass Spec.*, 443, 61
- Pradhan A. K., Nahar S. N., 2011, *Atomic Astrophysics and Spectroscopy*. Cambridge Univ. press, New York
- Seaton M. J., 1962, in Bates D. R., ed., *Atomic and Molecular Processes*. Academic Press, New York, p. 375
- Seaton M. J., 1975, *Adv. At. Mol. Phys.*, 11, 83
- Sitnova T. M., Mashonkina L. I., 2018, *Astron. Lett.*, 44, 411
- Storey P. J., Zeippen C. J., 2000, *MNRAS*, 312, 813
- Tayal S., Zatsarinny O., 2016, *Phys. Rev. A*, 94, 042707
- The Opacity Project Team, 1995, *The Opacity Project Vol. 1*, Institute of Physics Publications, Bristol
- van Regemorter H., 1962, *ApJ*, 136, 906

This paper has been typeset from a $\text{\TeX}/\text{\LaTeX}$ file prepared by the author.